Published by IOP Publishing for Sissa Medialab

Received: *February 7, 2024*
Accepted: *April 26, 2024*
Published: *May 21, 2024*

Characterisation of resistive MPGDs with 2D readout

L. Scharenberg,[a,*] **F. Brunbauer,**[a] **H. Danielsson,**[a] **Z. Fang,**[b,c] **K. J. Flöthner,**[a,d] **F. Garcia,**[e] **D. Janssens,**[a,f,g] **M. Lisowska,**[a,h] **J. Liu,**[b,c] **Y. Lyu,**[b,c] **B. Mehl,**[a] **H. Muller,**[a,i] **R. de Oliveira,**[a] **E. Oliveri,**[a] **G. Orlandini,**[a,j] **D. Pfeiffer,**[k,a] **O. Pizzirusso,**[a] **L. Ropelewski,**[a] **J. Samarati,**[k,a] **M. Shao,**[b,c] **A. Teixeira,**[a] **M. van Stenis,**[a] **R. Veenhof,**[a] **Z. Zhang**[b,c] **and Y. Zhou**[b,c]

[a] *European Organization for Nuclear Research (CERN), 1211 Geneva 23, Switzerland*
[b] *State Key Laboratory of Particle Detection and Electronics, University of Science and Technology of China, Hefei 230026, China*
[c] *Department of Modern Physics, University of Science and Technology of China, Hefei 230026, China*
[d] *Helmholtz-Institut für Strahlen- und Kernphysik, University of Bonn, Nußallee 14-16, 53115 Bonn, Germany*
[e] *Helsinki Institute of Physics, University of Helsinki, P.O. Box 64, FI-00014 Helsinki, Finland*
[f] *Inter-University Institute For High Energies, Pleinlaan 2, 1050 Brussels, Belgium*
[g] *Vrije Universiteit Brussel, Pleinlaan 2, 1050 Brussels, Belgium*
[h] *Université Paris-Saclay, F-91191 Gif-sur-Yvette, France*
[i] *Physikalisches Institut, University of Bonn, Nußallee 12, 53115 Bonn, Germany*
[j] *Friedrich-Alexander-Universität Erlangen-Nürnberg, Schloßplatz 4, 91054 Erlangen, Germany*
[k] *European Spallation Source ERIC (ESS), Box 176, SE-221 00 Lund, Sweden*

E-mail: lucian.scharenberg@cern.ch

Abstract: Micro-Pattern Gaseous Detectors (MPGDs) with resistive anode planes provide intrinsic discharge robustness while maintaining good spatial and time resolutions. Typically read out with 1D strips or pad structures, here the characterisation results of resistive anode plane MPGDs with 2D strip readout are presented. A μRWELL prototype is investigated in view of its use as a reference tracking detector in a future gaseous beam telescope. A MicroMegas prototype with a fine-pitch mesh (730 line-pairs-per-inch) is investigated, both for comparison and to profit from the better field uniformity and thus the ability to operate the detector more stable at high gains. Furthermore, the measurements are another application of the RD51 VMM3a/SRS electronics.

Keywords: Micropattern gaseous detectors (MSGC, GEM, THGEM, RETHGEM, MHSP, MICROPIC, MICROMEGAS, InGrid, etc); Gaseous imaging and tracking detectors; Electronic detector readout concepts (gas, liquid)

ArXiv ePrint: 2402.03899

*Corresponding author.

https://doi.org/10.1088/1748-0221/19/05/P05053

Contents

1 Introduction

In recent years, various experiments and detector R&D lines started the use of Micro-Pattern Gaseous Detectors (MPGDs) with resistive elements, mainly because of their discharge robustness [1–4]. Additionally, parameters such as the signal induction, i.e. the spread of the charge over a given number of readout channels, and rate-capability can be tuned to the desired values of the experiment by adjusting the design of resistive elements. This is most prominently employed in MPGDs with a single amplification stage, such as MicroMegas (MM) [5] and µRWELL [6].

In this paper, the results of a characterisation of these two technologies are shown. The studies are conducted in view of various R&D aspects. The first aspect is focused on the readout structure. So far, most MPGDs with continuous resistive layers employ either 1D-strips or pad structures [2] separated from the resistive layer. Here, the results for detectors with 2D-X-Y-strips underneath the resistive layer are presented. The second aspect is specific to the µRWELL detector that has been investigated. It is a prototype intended for use as a reference detector in a new additional third beam telescope for particle trajectory reconstruction of the DRD1 collaboration [7, 8] — the preceding RD51 collaboration [9, 10] provides for its joined test beam campaigns at the H4 beam line of CERN's SPS two beam telescopes, one based on MicroMegas and one based on triple-GEM detectors [11]. This prototype detector was also investigated in terms of the charge sharing between the two strip layers underneath the DLC — a previous prototype with 2D-X-Y-strip readout showed good performance [12] but an unequal signal sharing between the two strip layers. For the new prototype, this imbalance has been addressed by reducing the strip width of the top strips from 80 µm to 60 µm and reducing the insulating layer between the strip layers from 50 µm to 25 µm (for more details on the detector geometry see section 2.1 and figure 1). The third point is specific to the investigated MicroMegas detector. The particular detector is equipped with a fine mesh in the amplification stage with 730 line-pairs-per-inch (LPI), corresponding to a mesh cell pitch of 35 µm. The motivation for investigating a mesh structure like

2024 JINST 19 P05053

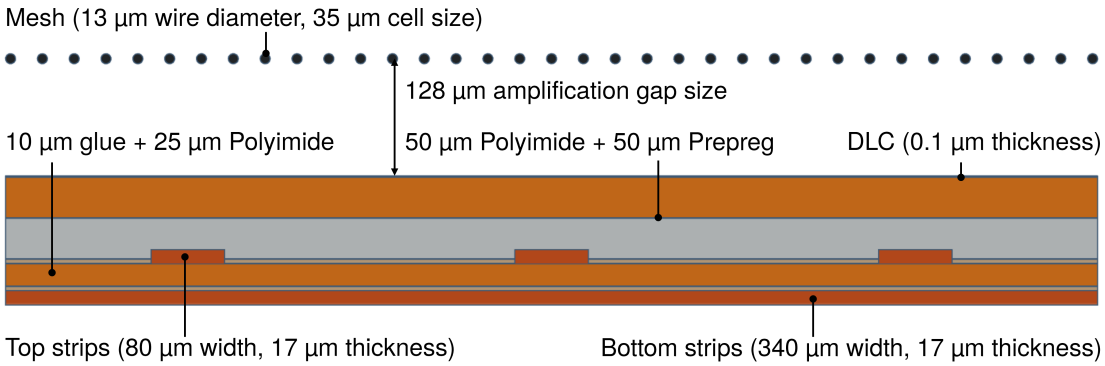

(a) MicroMegas

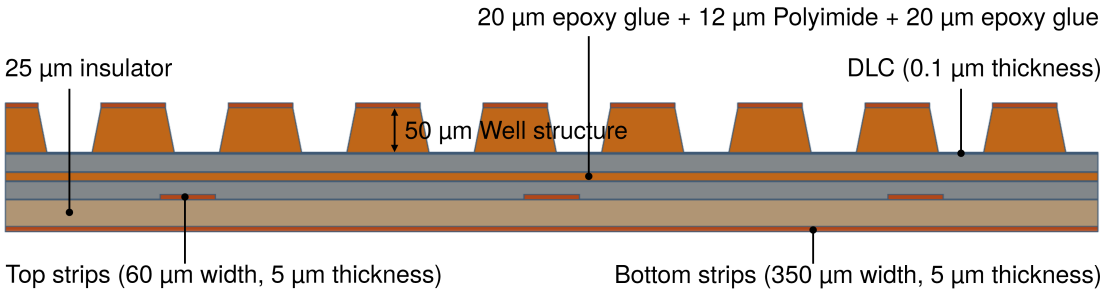

(b) µRWELL

Figure 1. Sketched cross-section of the MicroMegas (a) and the µRWELL (b) amplification stages, as used in the here presented measurements.

this is a more uniform electric field and thus the possibility to operate the detector at higher gains. While the stability measurements are part of a separate study — here only the results on the spatial resolution, time resolution and charge behaviour are presented — it can be noted that the MicroMegas detector could be operated at gains more than twice as high as the µRWELL detector. Another more general aspect is the use of the VMM3a front-end Application-Specific Integrated Circuit (ASIC) [13] together with the RD51 Scalable Readout System (SRS) [14] with a wider range of detectors.

2 Experimental methods

2.1 Devices under test

The gas mixture used to operate the detectors is Ar/CO_2 (70/30 %). Both detectors (sketched in figure 1) have an active area of $10 \times 10\,\mathrm{cm}^2$ with a 2D X-Y-strip readout with 256 strips in each direction. The strip pitch is 400 µm. In both detectors, the anode is a layer of Diamond-Like Carbon (DLC) with similar surface resistivities — 40 MΩ/sq for the µRWELL and 37 MΩ/sq for the MicroMegas. The drift region of each detector had a width of 3 mm. Although both detectors were operated with a negative high voltage on the cathode, the MicroMegas detector was operated with a grounded mesh

2024 JINST 19 P05053

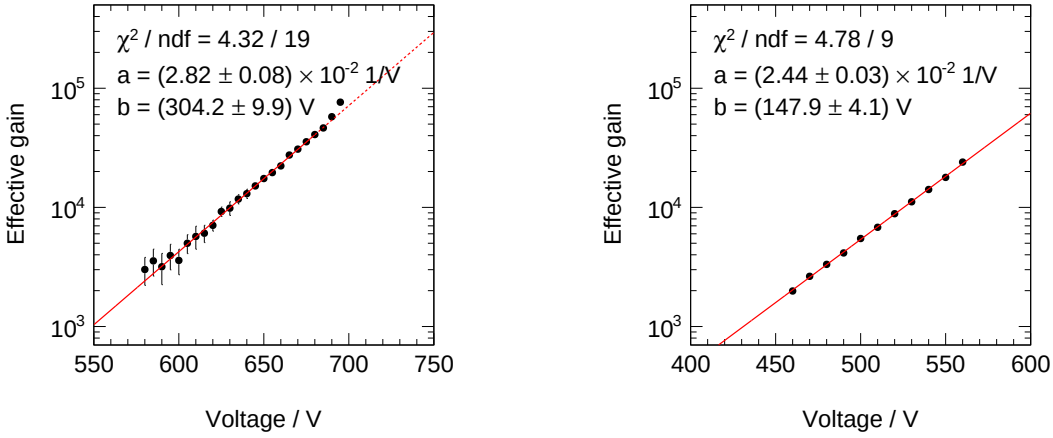

(a) MicroMegas (b) µRWELL

Figure 2. Gain curves of the (a) MicroMegas and the (b) µRWELL detector, obtained from measuring the signal current on the DLC layer. The solid line shown in (a) covers the fit range, while the dashed line is an extrapolation not included in the fit.

and a positive high voltage on the DLC anode, while the µRWELL was operated with a negative high voltage at the top layer of the Well structure and a grounded DLC anode.

When performing gain scans, the drift field was kept constant at around 2.4 kV/cm for the µRWELL, which corresponds to 724 V difference between the drift cathode and Well, and 0.9 kV/cm for the MicroMegas detector, which corresponds to 275 V between cathode and mesh. During the test beam measurements, the amplification voltages were varied from 460 to 570 V for the µRWELL and 580 to 700 V for the MicroMegas — at higher voltages, the detectors started to show instabilities in operation due to discharges leading to high voltage trips. Beforehand, a gain calibration was performed with an ^{55}Fe radioactive X-ray source to relate the effective gain G_{eff} of the detectors with the applied amplification voltage V. The effective gain itself is determined for each voltage point from the current measured on the DLC layer I_{DLC} by

$$G_{\text{eff}} = \frac{I_{\text{DLC}}}{N_0\, e\, f_{\text{i}}}\,, \tag{2.1}$$

with N_0 being the number of primary ionisation electrons, e the elementary charge and f_{i} the rate of interacting X-ray photons. Fitted to the data (figure 2) is an exponential function

$$G_{\text{eff}}(V) = \exp\big[a(V-b)\big]\,, \tag{2.2}$$

to obtain the final calibration curve.

When performing drift scans, the amplification voltage was kept constant at 680 V for the MicroMegas, which corresponds to an effective gain of around 40 000 at 0.9 kV/cm drift field, and at 540 V for the µRWELL, which corresponds to a gain of around 15 000 at 2.4 kV/cm drift field.

2.2 Beam telescope and readout electronics

Both detectors have been characterised as Devices Under Test (DUTs) with the RD51 VMM3a/SRS beam telescope [11]. It consists of three COMPASS-like triple-GEM detectors [15] with an active

2024 JINST 19 P05053

area of $10 \times 10\,\mathrm{cm}^2$ almost equally spaced with a total lever arm of around 1 m to provide the position information. In addition, it contains three scintillators with Photo-Multiplier Tubes (PMTs) connected to a NIM coincidence unit as a time reference. Similar to the DUTs, also the GEM detectors have been operated with Ar/CO_2 (70/30 %).

For the readout of the detectors, including the output of the NIM coincidence unit, the ATLAS/BNL VMM3a front-end ASIC [13] in its integration [16, 17] of the RD51 Scalable Readout System (SRS) [14] has been used. It provides the acquired charge per channel (10-bit ADC, effectively 7-bit) in a continuous, multi-channel self-triggered readout mode with around 1 ns time resolution and a MHz rate-capability. The adjustable analogue front-end parameters of the VMM3a have been set to 200 ns peaking time, 9 mV/fC electronics gain and around 10 000 electrons threshold per channel for both the DUTs and the reference detectors. The threshold level might seem high, but it should be considered that the VMM3a is operated in its self-triggered readout, meaning that each signal above the Threshold Level (THL) will be processed and become part of the data stream, i.e. a THL that is set too low will results in a lot of external pick-up noise being part of the raw data.

To reconstruct the acquired data, two software tools were used. The first step is the cluster reconstruction with *vmm-sdat* [18] on each strip plane individually. From the continuous data stream of the readout system, it first finds all signals within a predefined time window — set to 700 ns length — under the condition that the time difference between two consecutive hits is not larger than 350 ns. Within these so-called 'time clusters', the geometrical clustering is performed, allowing one missing strip between the hits. For more details on this procedure see [18, 19]. The second step is the event-building followed by the track reconstruction within the events. For this *anamicom* [20, 21] is used. The event building finds all the previously reconstructed clusters that are within a predefined time window — it was set to 2500 ns length, which was regarded as acceptable, considering an expected event rate of 50 kHz. For a detailed description of the event-building procedure see [19]. Within each event, the track finding and fitting are performed with a Kalman filter [22], which is described in detail in [23]. Both, for the studies on the efficiency of the DUTs (figure 4(b)) and their spatial resolution (section 4) it is required that the clusters in the DUT are part of the track finding. However, they are excluded from the track fit to not bias the spatial resolution results.

3 Charge and efficiency behaviour

With the previous µRWELL prototype showing an imbalance of the charge collection between the top and the bottom readout strips [12], the first point of investigation is the charge sharing and collection behaviour of the detectors. For this, the charge distribution (Landau distribution) is generated from all recorded interactions that can be assigned to a reconstructed particle trajectory from the beam telescope. Then the mean value of this measured distribution is taken and plotted depending on the effective gain of the detector (figure 3(a)). It can be seen that both strip planes collect almost the same amount of charge, resulting in a charge-sharing ratio between the top and bottom strips of each detectors close to one. Another observation is that the mean charge measured with the Landau distribution increases linearly with the gain for the µRWELL detector, while for the MicroMegas detector, the increase starts to flatten out at higher gains. This is due to the ADC saturation of individual readout channels which at higher gains is more likely to occur.

Another observation is that the total collected charge for the µRWELL is significantly less than for the MicroMegas detector, despite the same effective gain. A similar behaviour can be also observed

2024 JINST 19 P05053

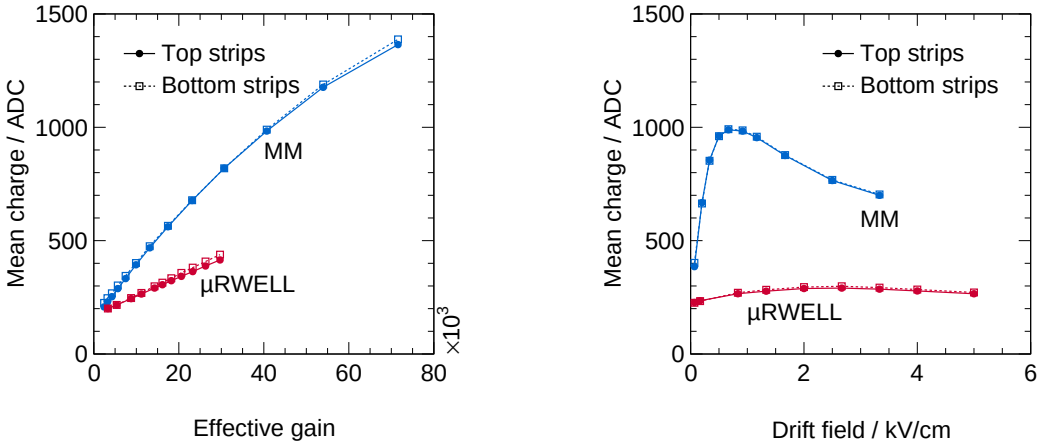

(a) Gain dependence (b) Drift field dependence

Figure 3. Average measured charge, i.e. the calculated mean of the energy loss distribution after amplification, depending (a) on the effective gain of the two investigated detectors or (b) on the drift field, in each read out detector plane.

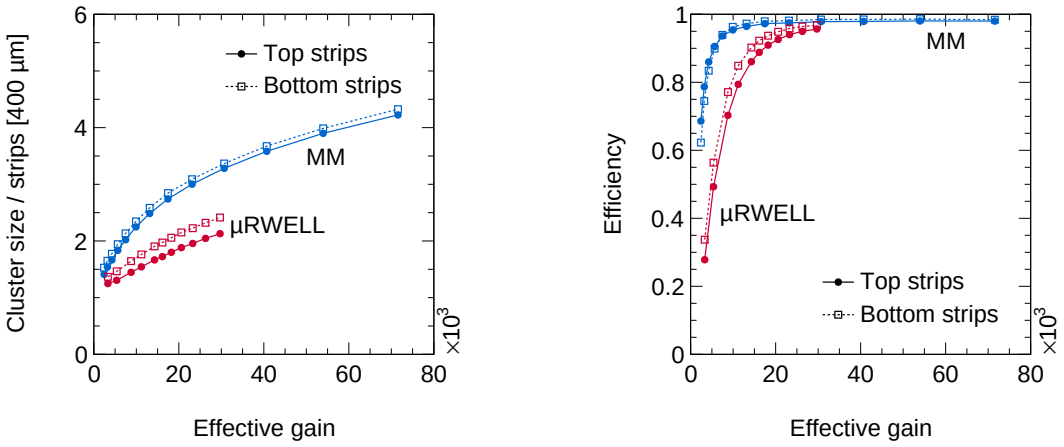

(a) Average cluster size (b) Detector efficiency

Figure 4. In (a), the mean of the cluster size distribution (distribution of the number of channels above the THL for each recorded interaction) is shown, depending on the effective gain of the detectors. In (b), the detector efficiency as defined in eq. (3.1) is shown, depending on the effective gain.

for the cluster size (number of channels above the THL), with the mean cluster size being plotted against the effective detector gain (figure 4(a)). It can be seen that the cluster size and the mean of the measured Landau distribution scale accordingly, with the bottom strips of the µRWELL collecting slightly more charge, also having a slightly larger cluster size, as well as an almost doubled cluster size for the MicroMegas detector at similar gains, with almost twice the amount of measured charge.[1] This

[1]In order to identify possible explanations for the observed difference, various simulation studies have been performed. However, as the simulations did not point in a specific direction, a full comparison of the two detectors in simulation is required. As this would overload the current work, the authors decided to simply report the observations and keep the

2024 JINST 19 P05053

behaviour is also reflected in the detector efficiency (figure 4(b)), which is defined as

$$\epsilon_{\text{det}} = \frac{N_{\text{det}}}{N_{\text{tracks}}} \,. \tag{3.1}$$

Here, N_{tracks} is the number of particle tracks reconstructed, using only the reference tracking detectors. This corresponds to the number of interactions expected within the DUT. It is compared with N_{det}, which is the number of tracks that include a cluster within the DUT.

Due to the difference between the investigated μRWELL and MicroMegas detectors, reflected by the smaller cluster size and mean value of the Landau distribution for the μRWELL, higher detector gains are needed to reach comparable cluster sizes and signal charges and thus comparable efficiencies. The maximum efficiencies that are reached are around 98 % for the MicroMegas — within the plateau region (see figure 4(b)) — and around 96 % for the μRWELL, which did not reach the plateau region. The reason for the deviation from 100 % efficiency of the MicroMegas is caused by two geometrical effects: the detector was slightly misaligned by around 3 mm, i.e. partially outside of the telescope's active area, as well as one of the front-end channels was not working.

From the observed differences in the signal charge between MicroMegas and μRWELL it is, important to note that while the effective detector gain was determined from the current measured on the resistive anode layer, the front-end electronics only measures the induced current in the capacitively coupled readout strips. Hence, the gain at which a discharge might occur in the detector is the one determined via the signal current on the anode plane.

In addition to the dependence on the effective gain of the detector, also the dependence of the measured charge depending on the electric drift field was studied, representing the charge collection behaviour by the amplification stage. The results are shown in figure 3(b). Both detectors show a charge collection behaviour, which was as also observed in the work of other groups: the μRWELL has a much broader peak at higher drift fields (e.g. as shown in [6]), while the MicroMegas shows a more well define peak at lower drift fields (e.g. as shown in [21]).

4 Spatial resolution

4.1 Basic results

The spatial resolution of the DUTs is extracted from the width of the residual distributions that are generated from the difference $\Delta x = x_{\text{ref}} - x'$ between the reference particle position x_{ref} that is provided by the reconstructed trajectory from the reference tracking detectors and the interaction point x' reconstructed in the DUTs. To determine the width, two overlapping Gaussian functions are fitted to the residual distribution, with the mean value being identical, but a weight factor w to account for the different scales and different standard deviations σ to account for the core and the tails of the residual distribution. The final width is thus defined as

$$\sigma^2_{\Delta x} = w\sigma^2_{\text{core}} + (1-w)\sigma^2_{\text{tail}} \,. \tag{4.1}$$

The spatial resolution is then obtained by quadratically subtracting the contribution from the uncertainty on the track reconstruction, as described in [19, 21, 24].

Using the Centre-Of-Gravity (COG) to determine the position of the particle interaction within the detector, the gain dependence of the spatial resolution as shown in figure 5(a) is obtained. For

simulation studies subject to a separate paper.

2024 JINST 19 P05053

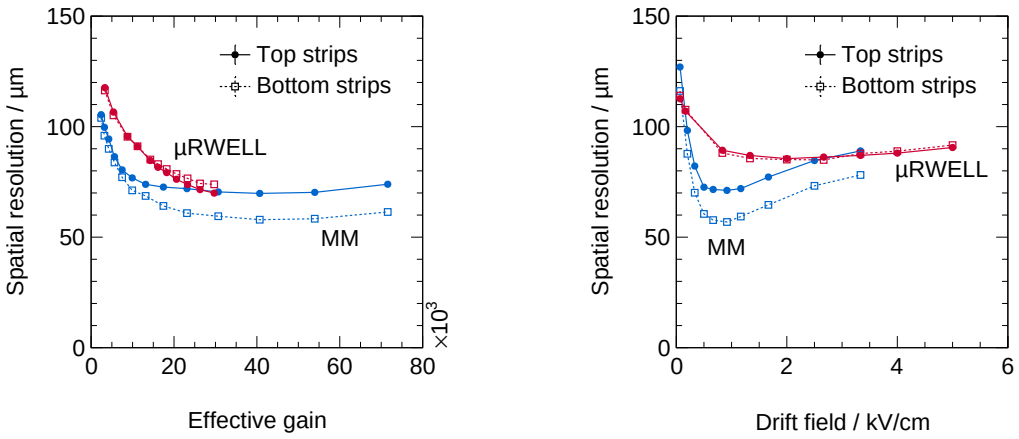

(a) Gain dependence

(b) Drift field dependence

Figure 5. Dependence of the spatial resolution of the two DUTs on (a) their effective detector gain and on (b) the electric drift field, determined for both readout planes individually.

both detectors, the spatial resolution improves with increased detector gain. Taking the cluster size behaviour (figure 4(a)) into account, this is related to more charge information being available and distributed over more than a single readout strip. This also explains the better spatial resolution of the MicroMegas compared to the µRWELL, as it has a larger charge collection and cluster size. A similar dependence can be observed when plotting the drift behaviour (figure 5(b)). The spatial resolution is inversely proportional to the charge collection depending on the electric drift field (figure 3(b)), i.e. the more charge collected, the better the spatial resolution.

At very high gains (figure 5(a)), the spatial resolution starts to decrease for the MicroMegas detector. This is due to the saturated readout channel that also caused the flattening of the measured charge-gain-dependence (figure 3(a)). The position reconstruction by COG loses accuracy when the relative amount of charge is not correctly represented anymore because the corresponding readout channel is in saturation.

Another observation is that the spatial resolution for the µRWELL is almost the same for the two readout planes, as it is expected from equal charge sharing, while for the MicroMegas the behaviour between the top and bottom strips deviates. This was found to be the result of the so-called 'readout modulation', as illustrated by figure 6. It shows the distribution of the reconstructed interaction points with high granularity. This makes a peak structure visible which originates from the readout pattern modulated into the position distribution that is expected to be uniform due to the detector's uniform irradiation. Due to this modulation effect by the discrete readout structure in combination with a threshold-based zero-suppressed readout electronics, the interaction points are more likely to be reconstructed to the central strip for odd-strip-count clusters and in-between the two central strips for even-strip-count clusters. For a more detailed description of this effect please refer to [25], while it should be noted that the effect has already been observed with Multi-Wire Proportional Chambers [26]. This behaviour affects the accuracy of the position determination, with a stronger effect leading to a worse spatial resolution. This is what can be deduced from figure 6, where the modulation effect is stronger for the top strips than for the bottom strips. It seems to be an intrinsic behaviour of the detector as it is also observed in laboratory measurements using an ^{55}Fe source.

2024 JINST 19 P05053

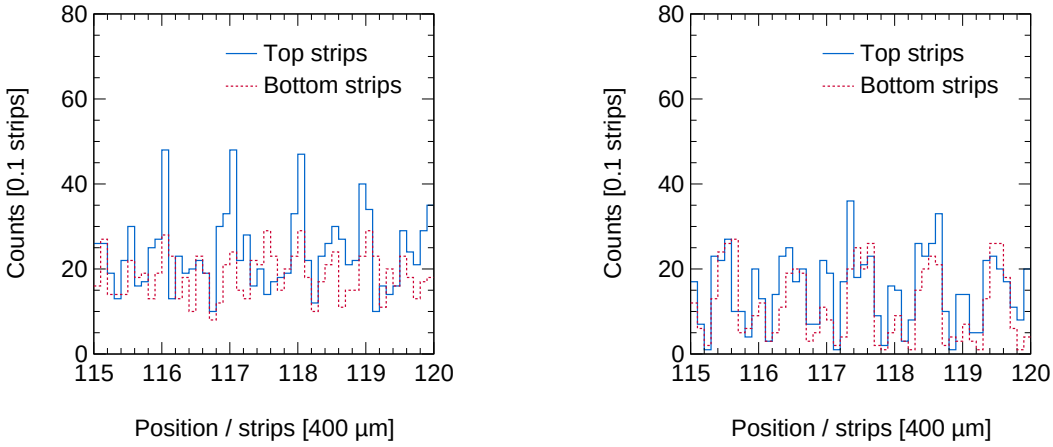

(a) High gain, approximately 40 000

(b) Low gain, approximately 8000

Figure 6. Distribution of the reconstructed interaction points at high granularity for the MicroMegas detector at high detector gains (a) and low detector gains (b).

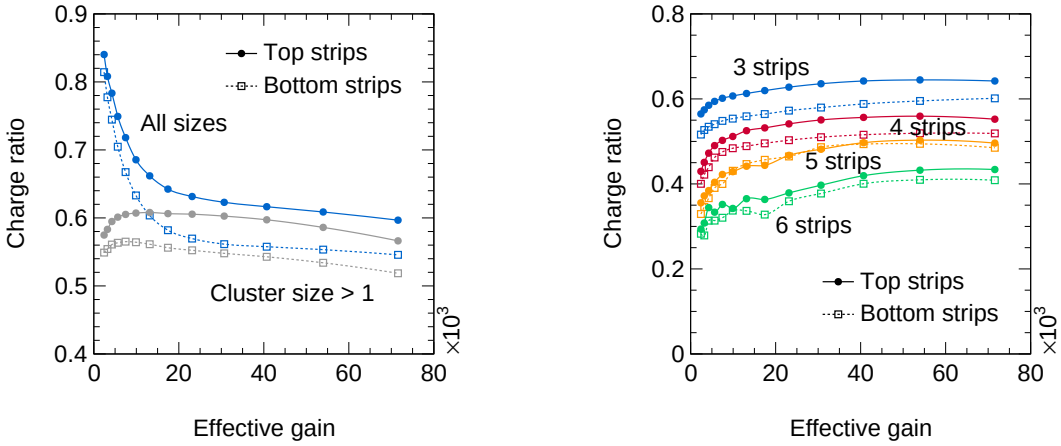

(a) All cluster sizes

(b) Selected cluster sizes

Figure 7. Average ratio between the charge of the strip with the highest amplitude within a cluster and the total cluster charge. In (a) this is shown for all cluster sizes, as well as all cluster sizes that are larger than one strip. In (b) it is shown for specifically selected cluster sizes.

A possible explanation that was found for this behaviour is the way the signal is induced. With the top strips being much thinner than the bottom strips, the distribution of the induced signal charge changes compared to the bottom strips, with more charge being in the cluster's central strip for the top strips and less charge being acquired in the outer strips. This explanation is underlined by what is shown in figure 7. There, the average ratio between the charge of the strip i within the cluster that acquired most of the charge $Q_{i,\max}$ and the total cluster charge Q_{tot}:

$$\langle \kappa \rangle = \left\langle \frac{Q_{i,\max}}{Q_{\text{tot}}} \right\rangle . \tag{4.2}$$

It can be seen that the charge distribution is different, especially for the most probable cluster sizes

2024 JINST 19 P05053

with three and four strips, with the largest amplitude strip acquiring less of the total cluster charge in the bottom strip layer.

4.2 Improving the spatial resolution

While so far, the results have been obtained with COG to calculate the position, previous studies [11, 25] showed that a different weighting of the charge in the COG formula

$$x' = \frac{\sum_i Q_i^n x_i}{\sum_i Q_i^n} \tag{4.3}$$

with i the index of the readout strip with a signal above THL and n the weighting factor reduces the modulation effect and thus improves the spatial resolution. This is because of low amplitude signals in the tails of the charge distribution that go above the THL on one side of the charge distribution with respect to the centre of the cluster but not on the other one. Thus, a certain fraction of charge information to reconstruct the position is lost and the reconstruction of the interaction point is forced towards the signal above the THL. To reduce the weight of the charge distribution's tails and thus mitigate the bias in the calculation of the interaction point, $n > 1$ can be selected. In previous studies with triple-GEM detectors [11], $n = 2$ was used due to its simplicity and its proximity to the optimal solution obtained from simulation studies [27, 28]. Thus, it was investigated, if this Q^2 weighting can also be used to improve the spatial resolution of µRWELL and resistive MicroMegas detectors.

In addition, an orthogonal approach was investigated, making use of a hardware feature of the VMM3a front-end ASIC, its Neighbouring-Logic (NL). By default, the neighbouring-logic is turned off, but when enabled, the NL triggers the acquisition of an induced signal with an amplitude below the THL, if the neighbouring channel has a signal that surpasses the THL. This allows to obtain more charge information and thus to improve the reconstructed position.

The results of these two methods, including their combination, are shown in comparison with the COG reconstruction in figures 8, 9. It can be seen that the Q^2 weighting has a large impact and significantly improves the spatial resolution. This is in line with the previous results for GEM detectors. However, it was also found that for the top strips of the MicroMegas detector (figure 9(a)), the spatial resolution improves only at low gains, when the top and bottom strips behave similarly in the COG reconstruction. As soon as the gain increases and the top and bottom strips start to deviate, the spatial resolution with Q^2 becomes worse. Although this is a very specific case, it shows a known limit of the Q^2 reconstruction, identified previously by simulation studies [25]. In the case that a significant fraction of the cluster charge is contained in a single strip — which is the case for the top strips of the MicroMegas detector, as shown before (figure 7) — the Q^2 methods 'over-corrects' and thus the spatial resolution decreases.

Compared to the Q^2 reconstruction, the effect of the NL is only visible at low gains, i.e. at low efficiencies and low signal-to-threshold ratios, where the relative amount of collected charge on the total cluster charge is large, with a large fraction of the induced signal charge being still below the THL. At higher gains, this effect gets reduced, which is also reflected in the larger cluster size, i.e. on more channels a signal above THL was acquired. Thus, the tails of the measured charge distribution contain less induced signal charge and the probability of acquiring electronics noise increases. As a result, the spatial resolution decreases. These two outcomes on Q^2 and the NL are exactly in line with what has been observed in previous studies [11, 19].

2024 JINST 19 P05053

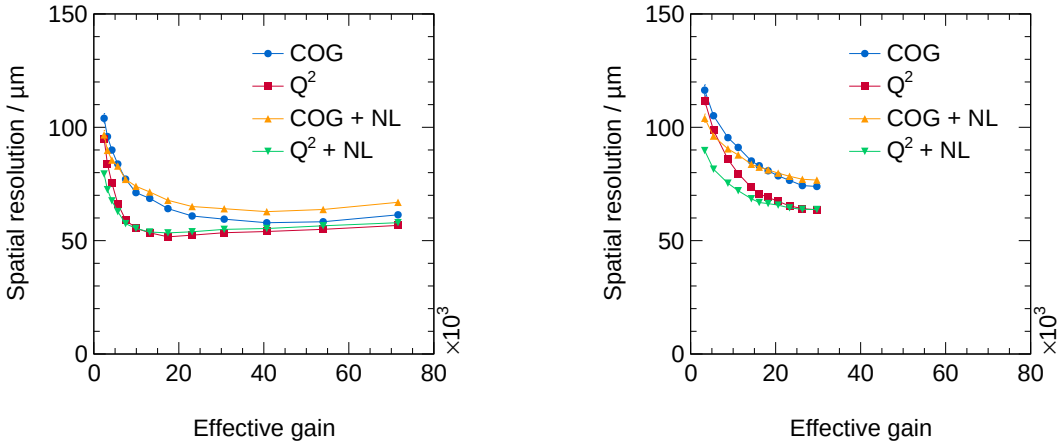

(a) MicroMegas (b) µRWELL

Figure 8. Dependence of the spatial resolution on the effective detector gain for the two different methods to determine the interaction point, with and without NL enabled. Here only the results of the bottom strips are shown. For a comparison with the top strips, see figure 9.

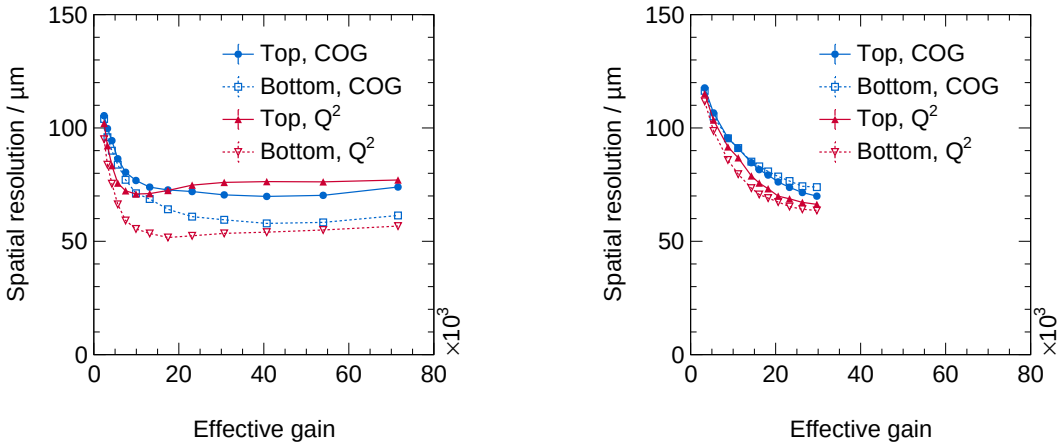

(a) MicroMegas (b) µRWELL

Figure 9. Comparison of the position resolution improvement with Q^2 weighting vs COG, for the top and bottom strips of both detectors, the MicroMegas (a) and the µRWELL (b).

5 Time resolution

As the last part of the characterisation studies, the time resolution of the two detectors is investigated. For this, the interaction time of the particle measured in the DUTs is compared with the reference time measured with the scintillator/PMT/NIM-coincidence-unit combination, both acquired with VMM3a/SRS. The reference time is provided as a constant amplitude signal by the NIM output of the coincidence unit on a single channel of the VMM3a. The measured interaction time in the DUTs is defined as

$$t' = \frac{1}{2}(t_{\text{top}} + t_{\text{bottom}}) \,. \tag{5.1}$$

2024 JINST 19 P05053

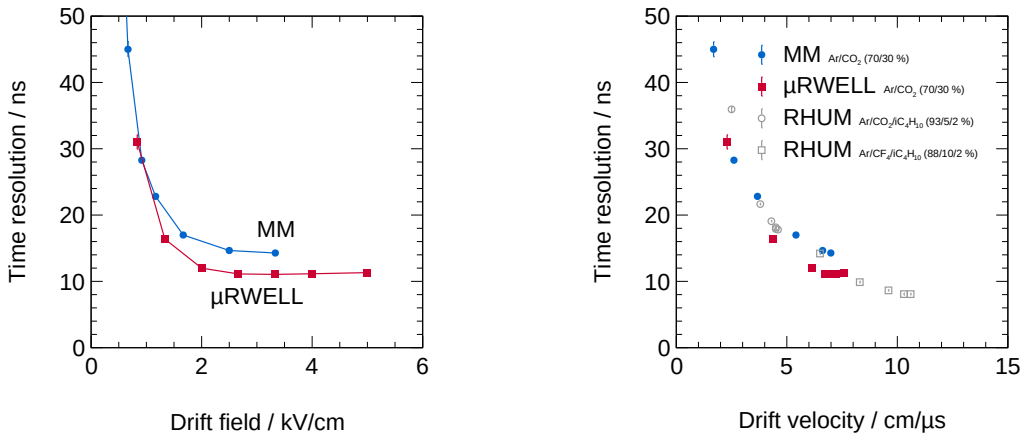

(a) Field dependence

(b) Velocity dependence

Figure 10. Measured time resolution for the two different detectors, depending on the electric drift field (a) and the electron drift velocity (b). For comparison purposes, also the results from measurements with a small-pad resistive MicroMegas detector from the RHUM project have been added [3].

The interaction timestamps for each plane, t_{top} and t_{bottom}, correspond to the time of the signal within each cluster with the largest peak amplitude.

With both timestamps found, their difference $\Delta t = t_{\text{ref}} - t'$ is calculated. Fitted to the resulting distribution is a single Gaussian function, with its width $\sigma_{\Delta t}$. The final time resolution is then this width, from which the time resolution contributions of the VMM3a (around 2 ns at the used peaking time of 200 ns) and the scintillator/PMT/NIM-logic (around 1.5 ns) are quadratically subtracted. The obtained time resolutions have been plotted against the electric drift field (figure 10(a)) and the electron drift velocity (figure 10(b)) which was calculated through Magboltz [29]. Added for reference, are data from measurements with a small-pad resistive MicroMegas detector from the RHUM project [3]. All data points show the same trend of an improved time resolution with increasing drift velocity. Two aspects should be noted though in regard to the used gas mixtures. The RHUM data have been obtained with a mixture of $Ar/CO_2/iC_4H_{10}$ (93/5/2 %) for the low drift velocities and $Ar/CF_4/iC_4H_{10}$ (88/10/2 %) for the high drift velocities ($> 6\,\text{cm}/\mu\text{s}$). In the case of the µRWELL, which has been filled with Ar/CO_2 (70/30 %), the drift velocity does not change significantly at fields above $2.5\,\text{kV}/\text{cm}$ — a linear increase of around $1\,\text{cm}/\mu\text{s}$ over a range of 2.5 kV. This explains the observed saturation behaviour of the time resolution. In the case of the MicroMegas detector, this saturation behaviour could not be observed, because of the high-voltage power supply, which did not allow it to go to larger drift voltages.

In addition to the observation that the time resolution in the three detectors follows the same trend and that the results are compatible with each other, two other points are shown by the measurements. Especially highlighted by the results from the resistive plane MicroMegas detector, it becomes clear that the working point for the best detector performance in terms of charge collection and spatial resolution (here at $0.9\,\text{kV}/\text{cm}$) is not necessarily the working point for the best time resolution (here $> 3\,\text{kV}/\text{cm}$), when the detectors are operated with Ar/CO_2 (70/30 %). Secondly, due to the capabilities of VMM3a/SRS, both types of detectors, as well as the reference timing detectors, could all be read out by the same front-end electronics, with the corresponding data being contained in a single data stream. This shows the versatility of the readout system, but also how it simplifies the data-taking

2024 JINST 19 P05053

and analysis process as it is not necessary to rely on additional high-precision timing electronics with an additional data stream that requires additional effort in the offline data analysis.

6 Conclusion and outlook

In this paper, the results from characterising two single-stage resistive plane MPGDs, a µRWELL detector and a MicroMegas detector, with 2D strip readout have been presented. Due to the capabilities of the new VMM3a/SRS readout electronics, it was possible to study simultaneously the charge behaviour, the spatial resolution and the time resolution of these two detectors.

One immediate observation was the difference in the amplitude of the induced signal measured by the front-end electronics between the two detectors, despite them being operated at the same gain. The full understanding of this behaviour requires simulation studies, which would go beyond the scope of this paper. However, it shows the importance of good signal development as otherwise, the detector efficiency can be still not sufficient although the detectors might be operated close to the breakdown voltages. Both detectors showed good performance though, which have been obtained using a gas mixture of Ar/CO_2 (70/30 %).

The µRWELL detector was investigated as a prototype detector for a future beam telescope of the DRD1 collaboration, in addition to the existing MicroMegas and GEM telescopes. With time resolutions of 10 ns, spatial resolutions of better than 70 µm and equal charge sharing between the two readout strip planes, the detector fulfils the requirements to be used in the new telescope. The MicroMegas detector was built with a 730 line-pairs-per-inch (LPI) mesh, corresponding to a mesh cell pitch of 35 µm, in order to increase the operation stability. Although the stability studies will be presented separately, the detector showed a good performance — e.g. spatial resolutions of around 50 µm — while being operated stably at gains of more than 50 000. In addition, the results demonstrated that in the chosen gas mixture the optimal working point to achieve the best spatial resolution and charge collection, is not necessarily the best working point to achieve the best time resolution.

Acknowledgments

This work has been supported by the CERN EP R&D Strategic Programme on Technologies for Future Experiments (https://ep-rnd.web.cern.ch/).

The detector production was fully financed by the CERN MPT workshop.

This project has received funding from the European Union's Horizon 2020 Research and Innovation programme under Grant Agreement No 101004761.

This work has been sponsored by the Wolfgang Gentner Programme of the German Federal Ministry of Education and Research (grant no. 13E18CHA).

The authors would like to thank Jona Bortfeldt (LMU Munich) for providing the anamicom software (https://gitlab.physik.uni-muenchen.de/Jonathan.Bortfeldt/anamicom) to reconstruct the particle trajectories.

The authors would also like to thank Maria-Teresa Camerlingo (INFN Bari), Paolo Iengo (INFN Napoli), Mauro Iodice (INFN Roma Tre) and Marco Sessa (INFN Roma Tor Vergata) for the exchange and discussions on the MicroMegas results and in particular for providing the RHUM reference data shown in figure 10.

2024 JINST 19 P05053

References

[1] T. Kawamoto et al., *New Small Wheel Technical Design Report*, Tech. Rep. CERN-LHCC-2013-006, CERN, Geneva, Switzerland (2013).

[2] D. Attié et al., *Characterization of resistive Micromegas detectors for the upgrade of the T2K Near Detector Time Projection Chambers*, *Nucl. Instrum. Meth. A* **1025** (2022) 166109 [arXiv:2106.12634].

[3] M. Iodice et al., *Towards large size pixelized Micromegas for operation beyond 1 MHz/cm^2*, 2023 *JINST* **18** C06029.

[4] G. Bencivenni et al., *The micro-RWELL detector for the phase-2 upgrade of the LHCb muon system*, *Nucl. Instrum. Meth. A* **1049** (2023) 168075.

[5] Y. Giomataris, P. Rebourgeard, J.P. Robert and G. Charpak, *MICROMEGAS: A high granularity position sensitive gaseous detector for high particle flux environments*, *Nucl. Instrum. Meth. A* **376** (1996) 29.

[6] G. Bencivenni, R. De Oliveira, G. Morello and M. Poli Lener, *The micro-Resistive WELL detector: a compact spark-protected single amplification-stage MPGD*, 2015 *JINST* **10** P02008 [arXiv:1411.2466].

[7] *DRD1 R&D* collaboration, *Development of Gaseous Detectors Technologies*, https://drd1.web.cern.ch/.

[8] A. Colaleo et al., *DRD1 Extended R&D Proposal*, Tech. Rep. CERN-DRDC-2024-003, CERN, Geneva, Switzerland (2024).

[9] RD51 collaboration, *Development of Micro-Pattern Gas Detectors Technologies*, https://rd51-public.web.cern.ch/

[10] M. Titov and L. Ropelewski, *Micro-pattern gaseous detector technologies and RD51 Collaboration*, *Mod. Phys. Lett. A* **28** (2013) 1340022.

[11] L. Scharenberg et al., *Performance of the new RD51 VMM3a/SRS beam telescope — studying MPGDs simultaneously in energy, space and time at high rates*, 2023 *JINST* **18** C05017 [arXiv:2302.08330].

[12] Y. Zhou et al., *Fabrication and performance of a μRWELL detector with Diamond-Like Carbon resistive electrode and two-dimensional readout*, *Nucl. Instrum. Meth. A* **927** (2019) 31.

[13] G. de Geronimo, G. Iakovidis, S. Martoiu and V. Polychronakos, *The VMM3a ASIC*, *IEEE Trans. Nucl. Sci.* **69** (2022) 976.

[14] S. Martoiu, H. Muller, A. Tarazona and J. Toledo, *Development of the scalable readout system for micro-pattern gas detectors and other applications*, 2013 *JINST* **8** C03015.

[15] C. Altunbas et al., *Construction, test and commissioning of the triple-GEM tracking detector for COMPASS*, *Nucl. Instrum. Meth. A* **490** (2002) 177.

[16] M. Lupberger et al., *Implementation of the VMM ASIC in the Scalable Readout System*, *Nucl. Instrum. Meth. A* **903** (2018) 91.

[17] L. Scharenberg et al., *Development of a high-rate scalable readout system for gaseous detectors*, 2022 *JINST* **17** C12014.

[18] D. Pfeiffer et al., *vmm-sdat — VMM3a/SRS Data Analysis Tool*, https://github.com/ess-dmsc/vmm-sdat.

[19] L.S. Scharenberg, *Next-Generation Electronics for the Read-Out of Micro-Pattern Gaseous Detectors*, Ph.D. thesis, Rheinische Friedrich-Wilhelms-Universität Bon, Bonn, Germany (2023), https://cds.cern.ch/record/2860765.

[20] J. Bortfeldt, *anamicom*

2024 JINST 19 P05053

[21] J. Bortfeldt, *Development of Floating Strip Micromegas Detectors*, Ph.D. thesis, Ludwig-Maximilians-Universität München, München, Germany (2014), https://cds.cern.ch/record/2632495.

[22] R.E. Kalman, *A New Approach to Linear Filtering and Prediction Problems*, *J. Basic Eng.* **82** (1960) 35.

[23] F. Klitzner, *Development of novel two-dimensional floating strip micromegas detectors with an in-depth insight into the strip signal formation*, Ph.D. thesis, Ludwig-Maximilians-Universität München, München, Germany (2019).

[24] S. Horvat, *Study of the Higgs Discovery Potential in the Process* $pp \to H \to 4\mu$, Ph.D. thesis, University of Zagreb, Zagreb, Croatia (2005), https://cds.cern.ch/record/858509

[25] L. Scharenberg et al., *X-ray imaging with gaseous detectors using the VMM3a and the SRS*, *Nucl. Instrum. Meth. A* **1011** (2021) 165576.

[26] F. Piuz, R. Roosen and J. Timmermans, *Evaluation of systematic errors in the avalanche localization along the wire with cathode strips readout MWPC*, *Nucl. Instrum. Meth.* **196** (1982) 451.

[27] H. Pulkkinen, *Basic properties of Gas Electron Multipliers and different methods to determine the cluster characteristics*, Student Report Tfy-3.5111, Aalto University, Espoo, Finland (2013).

[28] D. Janssens, *Resistive electrodes and particle detectors: Modeling and measurements of novel detector structures*, Ph.D. thesis, Vrije Universiteit Brussels, Brussels, Belgium (2024), https://cds.cern.ch/record/2890572

[29] S.F. Biagi, *Magboltz — transport of electrons in gas mixtures*, https://magboltz.web.cern.ch/magboltz/.

2024 JINST 19 P05053